Analytical Methods

ROYAL SOCIETY OF CHEMISTRY

PAPER

View Article Online
View Journal | View Issue

Cite this: *Anal. Methods*, 2023, **15**, 3577

An electrochemical immunosensor for an alpha-fetoprotein cancer biomarker on a carbon black/palladium hybrid nanoparticles platform

Foluke O. G. Olorundare,[a] Dimpo S. Sipuka,[ac] Tsholofelo I. Sebokolodi,[ac] Tetsuya Kodama,[b] Omotayo A. Arotiba *[ac] and Duduzile Nkosi*[ac]

The early detection of cancer is a key step in cancer survival. Thus, there is a need to develop low-cost technologies, such as electrochemical immunosensor technologies, for timely screening and diagnostics. The discovery of alpha-feto protein (AFP) as a tumour-associated antigen lends AFP as a biomarker for cancer detection and monitoring. Thus, immunosensors can be developed to target AFP in cancer diagnostics. Hence, we report the application of a hybrid nanocomposite of carbon black nanoparticles (CBNPs) and palladium nanoparticles (PdNPs) as a platform for the electrochemical immunosensing of cancer biomarkers. The hybrid carbon–metal nanomaterials were immobilised by using the drop-drying and electrodeposition technique on a glassy carbon electrode, followed by the immobilisation of the anti-AFP to fabricate an immunosensor. The nanoparticles were characterised with electron microscopy, voltammetry, and electrochemical impedance spectroscopy (EIS). Square wave voltammetry (SWV) and EIS were used to study the immunosensor signal toward the bio-recognition of the AFP cancer biomarker. The hybrid nanoparticles enhanced the immunosensor performance. A linear detection range from 0.005 to 1000 ng mL^{-1} with low detection limits of 0.0039 ng mL^{-1} and 0.0131 ng mL^{-1} were calculated for SWV and EIS, respectively. The immunosensor demonstrated good stability, reproducibility, and selectivity. Its real-life application potential was tested with detection in human serum matrix.

Received 5th May 2023
Accepted 30th June 2023

DOI: 10.1039/d3ay00702b

rsc.li/methods

1. Introduction

Globally, cancer is known as a precarious life-threatening disease.[1] In 2022, about 2 million new cancer occurrences and over 0.6 million deaths due to cancer were estimated in the USA.[2] Meanwhile, in other parts of the world, the prevalence of all cancers, especially in South Africa, is increasing progressively with over 0.1 million anticipated cases between 2019 and 2030.[3,4] While there is no definite cure for cancer, the chances of survival from cancer is positively associated with early diagnosis or identification. The early detection, screening, and predicting patient therapeutic response improve the efficiency of treatment and long-term survival of cancer patients.[5] Thus, more research in the direction of cancer diagnostics is urgently needed.

The discovery of biomarkers has been beneficial to cancer detection and monitoring.[6] Some biomarkers are indicators of the occurrences of different types of cancer.[5,7] For example, alpha-fetoprotein (AFP), is a glycoprotein synthesized by the fetal yolk sac and liver cells. AFP can be used to identify and predict certain types of tumours, such as teratoma endoderm, testicular cancer, ovarian cancer, squamous cell carcinoma of the cervix, yolk sac cancer, gastric cancer and hepatocellular cancer.[8,9] An increase in the concentration of AFP over 25 ng mL^{-1} can be an indication of cancer.[7,10,11] For the detection of AFP, methods such as chemiluminescent immunoassay (CLI),[12] enzyme-linked immunoassay (ELISA),[13] fluorescence immunoassay (FI),[14] electrochemiluminescence (ECL) immunoassay,[15] and surface plasmon resonance (SPR) immunoassay,[16] have emerged. Although the aforementioned methods have good sensitivity, they are usually expensive with complicated processes and have extensive analysis times. In comparison with these methods, electrochemical immunosensor technologies for the detection of cancer biomolecules or analytes have many advantages, such as low cost, high sensitivity, portability, negligible sample requirement, and the ease of operation.[17–19] In this light, electrochemical immunosensors are studied for cancer diagnostics.

Generally, electrochemical immunosensors can be labelled[20,21] or label free.[22,23] Electrochemical immunosensors based on label-free strategies have captivated attention in the detection of AFP, owing to its ease of preparation, ease of

[a]*Department of Chemical Sciences, University of Johannesburg, Doornfontein 2028, Johannesburg, South Africa. E-mail: oarotiba@uj.ac.za; dnkosi@uj.ac.za*
[b]*Laboratory of Biomedical Engineering for Cancer, Graduate School of Biomedical Engineering, Tohoku University, 4-1 Seiryo, Aoba, Sendai, Miyagi, 980-8575, Japan*
[c]*Centre for Nanomaterials Science Research, University of Johannesburg, South Africa*

detection, simplicity, very good accuracy, chemical stability, low cost and high biocompatibility.[24] In label-free immunosensors, signal enhancement strategies, such as the use of a hybrid electroactive and conductive nanomaterials as immobilisation layer for the bioreceptor–analyte biorecognition (antibody–antigen immunocomplex formation), are critical in obtaining low detection limits and augmenting the sensitivity of electrochemical immunosensor assays. Recently, different materials or composites have been reported to amplify the signal and enhance the sensitivity of electrochemical immunosensors for AFP detection.[25] For example, Wang *et al.*[19] reported the development of a novel electrochemical immunosensor on functionalized graphene nanocomposites (TB–Au–Fe_3O_4–rGO) in order to achieve a higher signal amplification for the detection of AFP, and obtained 2.7 fg mL^{-1} as the detection limit.[19] Furthermore, Wang *et al.*[26] invented a unique electrochemical immunosensor platform using a Cu_3PtNFs-catalysed oxygen reduction reaction (ORR) as signal amplification to detect AFP. A linear range of 0.1–104 pg mL^{-1} and a detection limit of 0.033 pg mL^{-1} was recorded. Using an aptamer, Upan *et al.*[11] developed an aptasensor on a platinum and graphene oxide platform with a limit of detection in the nanogram per mL concentration.[11]

The reactivity of an electrochemical immunosensor is considerably influenced by the conductivity/sensitivity of the sensors surface. Thus, various nanomaterials (NMs) comprising carbon materials, metal nanoparticles, metal oxides, quantum dots and others have been employed to modify electrodes in order to boost the immunosensor signal or performance.[27] Hybrid nanoparticles are particularly desirable due to their enhanced electrical properties, magnetic properties, optical properties, long-term stability, and chemical properties, which are superior to single-constituent nanoparticles.[28] In this work, a hybrid platform of carbon black and palladium nanoparticles was used for the development of an immunosensor for the first time.

Carbon black nanoparticles (CBNPs) are carbonaceous nanomaterials that are used because of their properties, which include dispersibility, high conductivity, high surface area and low cost. In addition to their resistance to fouling, CBNPs have the advantages of increasing electron transfer, improving sensitivity, and reducing the applied potential for analyte quantification.[29,30] They have also been found to be biocompatible owing to their low or non-toxicity.[31] CBNPs are spherical nanoparticles with the basal planes oriented parallel to the surface, and are known to possess a high surface area.[32] They also have surface groups with a high concentration of oxygen that may be involved in the covalent bonding to many biological receptors.[29] Good chemical stability and the high surface area of CBNPs make them good carriers or supports for metal nanoparticles.[30]

Owing to the properties of CBNPs, they have found application in electrochemical sensors and biosensor. For instance, Ławrywianiec *et al.*[33] utilized CBNPs to modify a glassy carbon electrode (GCE) for the detection of bisphenol A. The modified electrode significantly improved the oxidation peak current of bisphenol A compared with the bare GCE. A detection limit of 3.4×10^{-9} mol L^{-1} was obtained under optimum conditions.[33] Mazzaracchio *et al.*[28] reported on a fabricated electrochemical sensor based on CBNPs and a poly(propylene imine) (PPI)

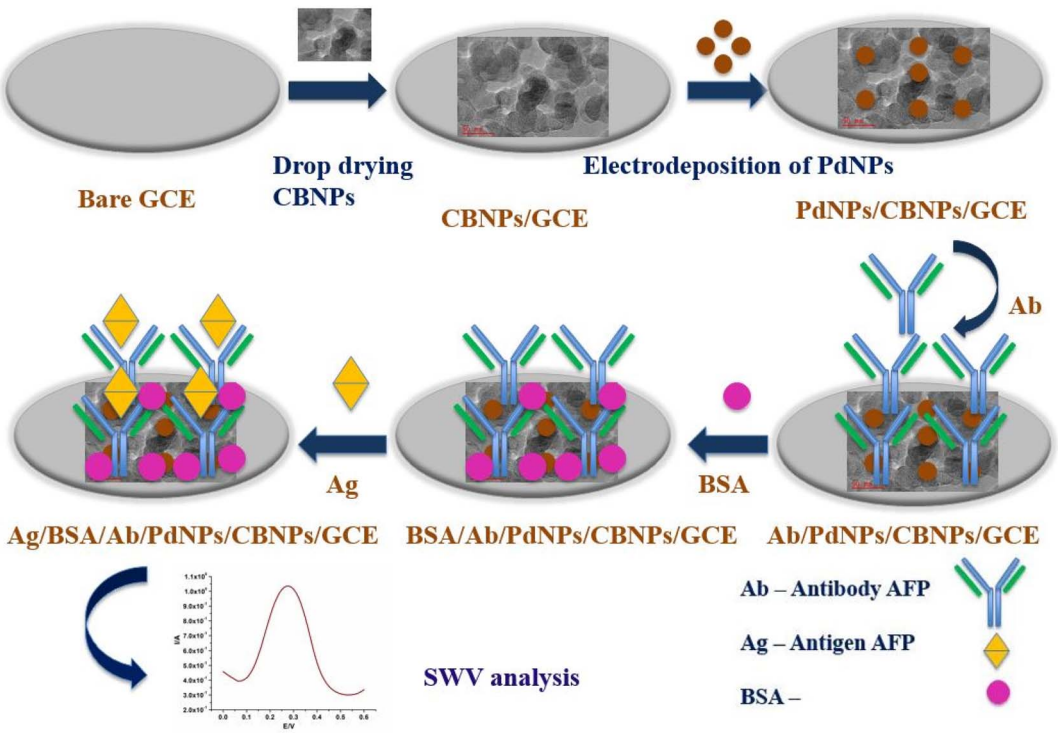

Scheme 1 Schematic diagram for the fabrication process of the immunosensor.

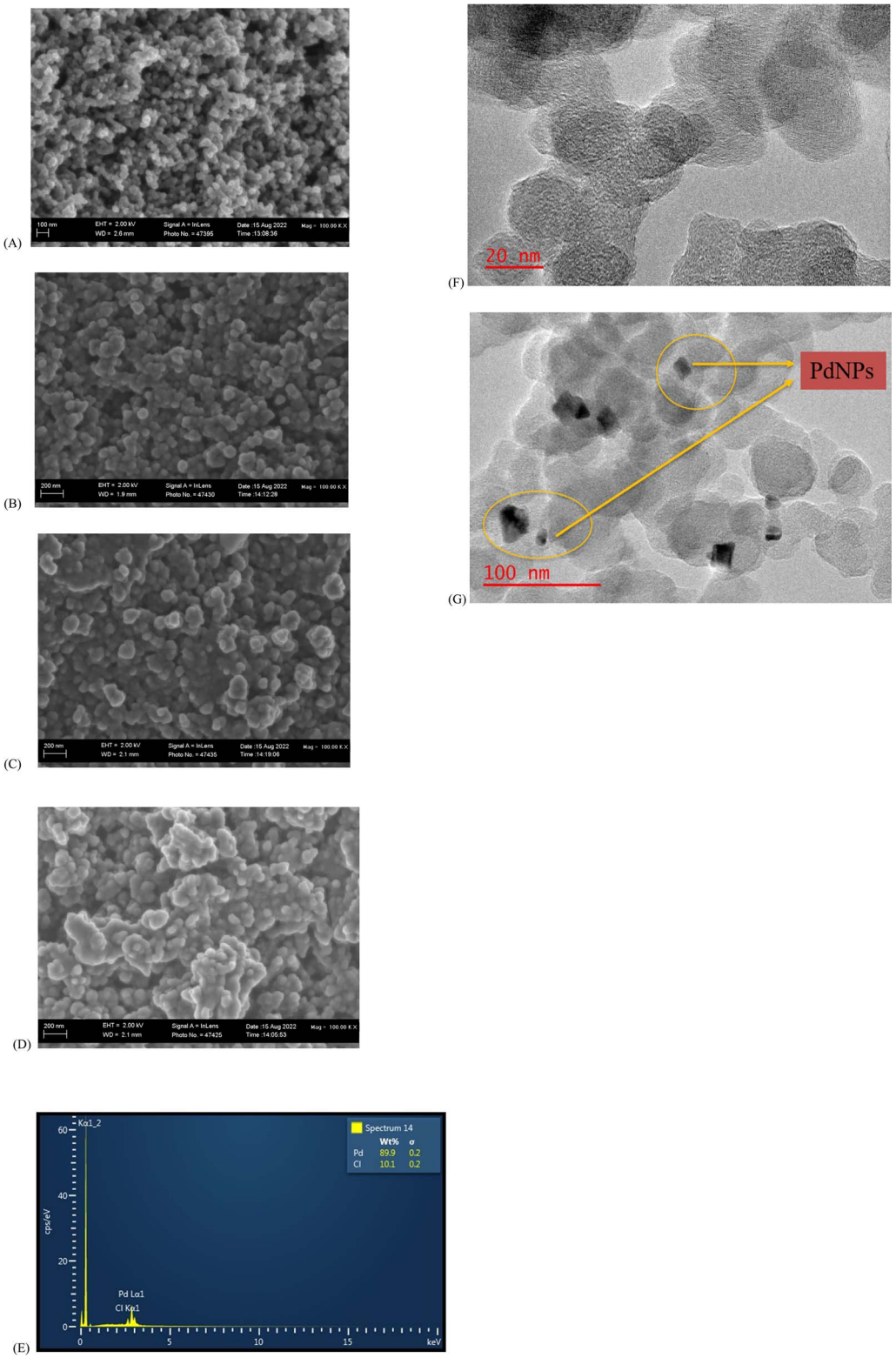

Fig. 1 FESEM micrographs of (A) CBNPs, (B) SPCE–CBNPs, (C) SPCE–PdNPs, (D) SPCE–CBNPs–PdNPs, and (E) EDS of CBNPs–PdNPs. TEM images of (F) CBNPs and (G) CBNPs/PdNPs.

Table 1 Cyclic voltammogram and impedance parameters of the immunosensor fabrication

Modified electrodes	I_{pa} (mA)	ΔE (mV)	R_s (Ω)	R_{ct} (Ω)	CPE (nF)
GCE	0.02	410	120.5	3102	60.17
GCE/CBNPs	0.23	120	93.84	139.1	15.94
GCE/CB/PdNPs	0.32	75	62.16	5.777	40.16
GCE/CBNPs/PdNPs/antibody	0.27	150	83.28	18.164	25.95
GCE/CBNPs/PdNPs/antibody/BSA	0.05	160	77.59	44.76	10.48

dendrimer on a screen-printed electrode (SPE) for the co-detection of lead and cadmium metallic ions in water. Low detection limits of 3.6 ppb and 15.3 ppb were obtained for the simultaneous detection of both metallic ions (lead and cadmium).[28]

The other material used in the hybrid immunosensor reported in this work is palladium nanoparticles (PdNPs). PdNPs have found application in electrochemical immunosensing nanotechnology development owing to their catalytic properties, good conductivity and high surface area.[32] The incorporation of PdNPs in the fabrication of the electrode surface improves the electron transfer, and also lowers the detection limit.[34] Furthermore, palladium-based metal nanoparticles with its excellent properties have been applied in the detection of cancer biomarkers, displaying properties such as ease of synthesis, diverse optical properties, and a range of adsorption sites for binding biological macromolecules, which are opened up for electrochemical immunosensing nanotechnology application.[35] PdNPs have been used as a hybrid component in electrochemical detection. For example, Jain *et al.*[36] fabricated an electrochemical biosensor for the detection of a neuromodulator level in biological samples using a hybrid of

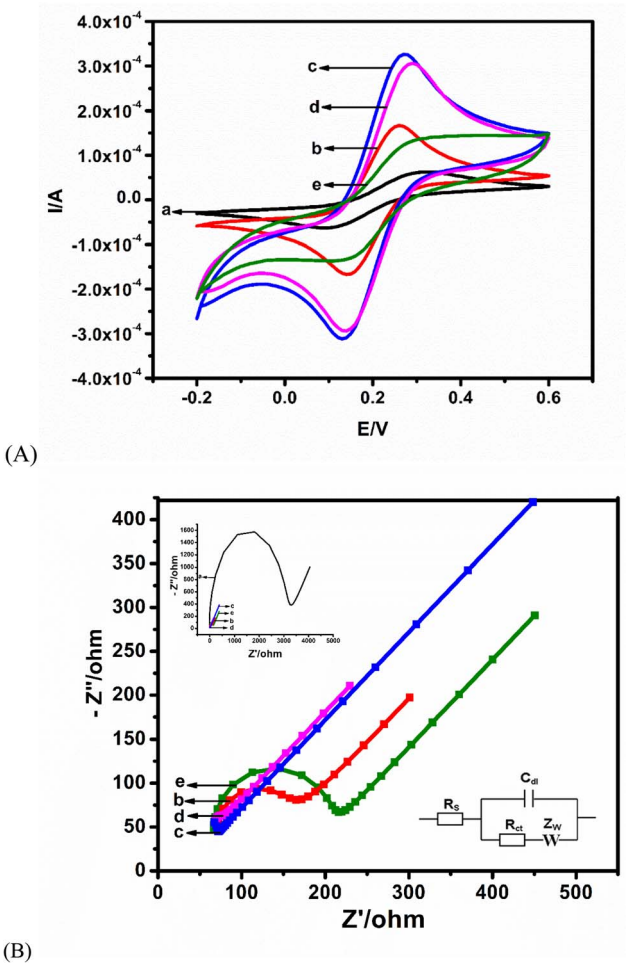

Fig. 2 (A) CV of (a) bare GCE, (b) CBNPs/GCE, (c) PdNPs/CBNPs/GCE, (d) antibody/PdNPs/CBNPs/GCE and (e) BSA/antibody/PdNPs/CBNPs/GCE in 5 mM $[Fe(CN)_6]^{3-/4-}$ in 0.1 M KCl. At (B) EIS of (b) CBNPs/GCE, (c) PdNPs/CBNPs/GCE, (d) antibody/PdNPs/CBNPs/GCE and (e) BSA/antibody/PdNPs/CBNPs/GCE in 5 mM $[Fe(CN)_6]^{3-/4-}$ in 0.1 M KCl. Inset shows the EIS of the frequency range = 100 KHz to 100 mHz; bias potential = 0.22 V.

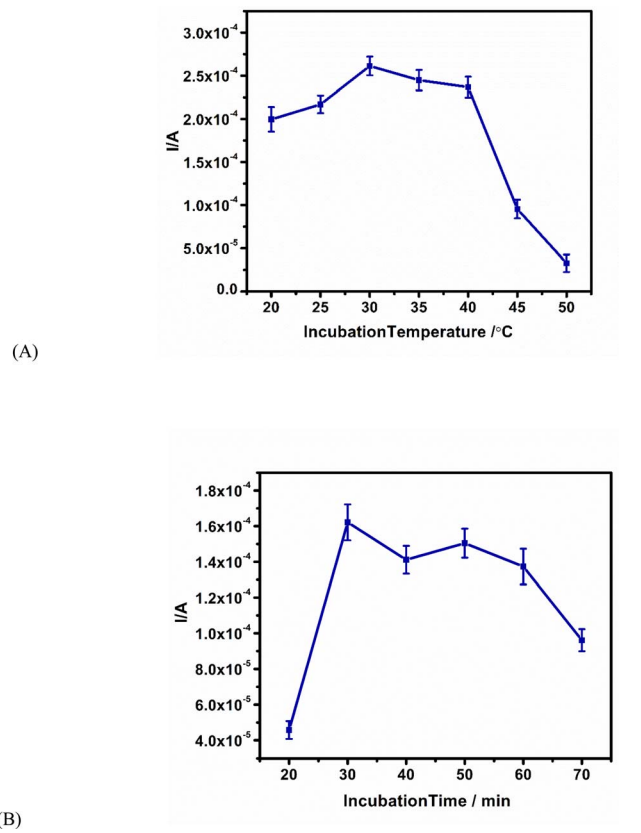

Fig. 3 Optimisation of the immunosensor in 100 ng per mL AFP antigen. (A) Incubation temperature from 20 °C to 50 °C. (B) Incubation time from 20 min to 70 min.

molybdenum disulfide nanostructures and PdNPs. In another work, a hybrid of a composite of PdNPs (as an electrocatalyst) with an amine-functionalized Cr-based organometallic framework (Pd/MIL101-NH_2) was used for the detection of telomerase.[37]

The use of hybrids as an immobilisation layer in biosensor development brings together the favourable properties of each of the components usually in a synergetic manner. Nanohybrids are used to tailor and enrich the desired immobilisation chemistry. For example, in an aptasensor for the detection of bisphenol A on a hybrid of a poly (propylene imine) dendrimer–carbon nanofiber, the dendrimer was used for supramolecular attachment of the dendrimer, while the carbon nanofiber was used to improve the conductivity of the electrode.[38] Mushiana *et al.*[39] reported on an electrochemical aptasensor for arsenic on a hybrid of carbon and gold nanoparticles. The carbon nanoparticle was used as a nano-template for the uniform immobilisation of gold nanoparticles by electrodeposition, while the gold nanoparticle was used to anchor a thiolated aptamer onto the electrode surface through Au–S linkage.[39] These two examples and others[28,36,37,40] show that hybrids can be used to improve the performance and stability of an electrochemical biosensor by improving the following properties: bioreceptor immobilisation, surface area, conductivity, electrocatalysis *etc.*

In this study, we explore a synergic combination of CBNPs and PdNPs as a nanohybrid to develop an electrochemical immunosensor for the detection of AFP. The carbon black and palladium nanoparticles were deposited on GCE to improve the analytical performance of the immunosensor for the AFP biomarker detection. The developed platform performance and application to a human serum sample were also investigated.

2. Experimental

2.1. Chemicals and instrumentation

Human serum, $K_3[Fe(CN)_6]$, $K_4[Fe(CN)_6]\cdot 3H_2O$, KCl, $KHPO_4$, KH_2PO_4, bovine serum albumin (BSA) (96–98%), ascorbic acid, D-glucose, urea, uric acid, dopamine, *N*,*N*-dimethylformamide (DMF) and carbon black nanoparticles were purchased from Merck Sigma-Aldrich, South Africa. Alpha-fetoprotein and anti-AFP (monoclonal), human epidermal growth factor receptor 2 (HER2), carcinoembryonic antigen (CEA) and prostate-specific antigen (PSA) were procured from Celtic Diagnostics (South Africa).

The chemicals used were of analytical grade, and used without further purification. Ultrapure Millipore water was utilized for all of the chemical preparations throughout the experiments with a resistivity of 18.2 MΩ cm at 24.1 °C from Merck Millipore, South Africa. Phosphate-buffer saline (PBS) of pH 7.5 was applied as an electrolyte for all experimental measurements.

2.1.1. Instrumentation. The electrochemical experiments were carried out on an Ivium compactstat potentiostat (Netherlands) using a GCE, Ag/AgCl (3 M NaCl) and platinum wire as the working, reference and counter electrodes, respectively. Electrochemical measurements were performed after degassing for 5 min with ultra-pure argon. Electron microscopy was

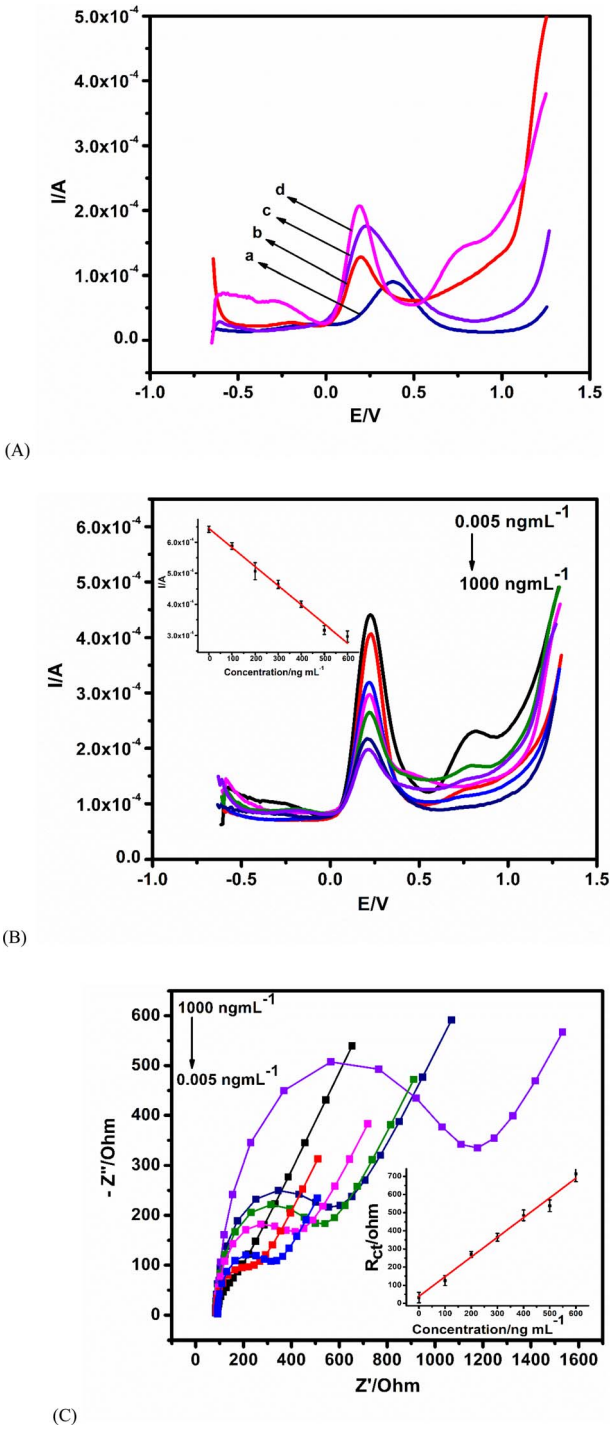

Fig. 4 (A) SWV of immunosensors on different platforms for the detection of 100 ng per mL antigen AFP: (a) GCE/antibodyAFP/BSA, (b) GCE/PdNPs/antibodyAFP/BSA, (c) GCE/CBNPs/antibodyAFP/BSA, and (d) GCE/CBNPs/PdNPs/antibodyAFP/BSA. (B) SWV of various concentrations of AFP from 0.005 to 1000 ng mL^{-1} in 5 mM ferri/ferrocyanide in 0.1 M KCl solution at pH 7.5 at 25 Hz. The calibration curve is the inset (error bar = SD (N = 3)). (C) EIS of different concentrations of AFP from 0.005 to 1000 ng mL^{-1} in 5 mM ferri/ferrocyanide in 0.1 M KCl solution at pH 7.5 at 25 Hz. The calibration curve is the inset (error bar = SD (N = 3)).

Table 2 Analytical performance of some immunosensors for AFP in the literature[a]

Immunosensor	Linear range (ng mL^{-1})	Detection limit	References
1. GNRs	0.1–200 ng mL^{-1}	0.04 ng mL^{-1}	41
2. (HBPE-NO_2)/CS–Au	0.1–120 ng mL^{-1}	0.055 ng mL^{-1} (DPV)	42
3. CNPs/AuNPs	0.005–1000 ng mL^{-1} & 0.00175 ng mL^{-1} (EIS)	0.0019 ng mL^{-1} (SWV)	40
4. AuNPs/G3PPI	0.005–500 ng mL^{-1} & 0.00185 ng mL^{-1} (EIS)	0.0022 ng mL^{-1} (SWV)	43
5. 3DOM IrO_x	1–250 ng mL^{-1}	0.3 ng mL^{-1} (CV)	24
6. AuNPs/PGNR	5–60 ng mL^{-1}	1 ng mL^{-1} (DPV)	44
7. PtNPs/GO-COOH	3.0–30 ng mL^{-1}	1.22 ng mL^{-1} (DPV)	11
8. CBNPs/PdNPs	0.005–1000 ng mL^{-1} & 0.0131 ng mL^{-1} (EIS)	0.0039 ng mL^{-1} (SWV)	Present work

[a] (1) Gold nanorods GNRs, (2) hyperbranched polyester nanoparticles with nitrite groups/chitosan/gold nanoparticles (HBPE-NO_2)/CS–Au, (3) carbon/gold bi-nanoparticles, CNPs/AuNPs, (4) gold nanoparticles/generation 3 poly(propylene imine) AuNPs/G3PPI, (5) three-dimensional ordered macroporous iridium oxides 3DOM IrO_x, (6) gold nanoparticles/porous graphene nanoribbon AuNPs/PGNR, (7) platinum nanoparticles on carboxylated graphene oxide PtNPs/GO-COOH.

carried out with field emission scanning electron microscopy (FESEM) on a Zeiss Crossbeam 540 FEGSEM incorporated with Oxford instruments energy dispersive X-ray spectroscopy (EDS) detector (Germany) and transmission electron microscopy (TEM) using JEOL JEM-2100F (Japan) with the energy dispersive X-ray (EDX).

2.1.2. Immunosensor preparation. The GCE was polished sequentially with an aluminum slurry of sizes 1.0, 0.3, and 0.05 μm, then washed with water and ethanol. CBNPs (10 mg) were dispersed in a blend of 5 mL of *N*,*N*-dimethyl formamide (DMF) and 5 mL of deionized water. The dispersion was sonicated for 1 h, drop-dried (20 μL) on the GCE, dried overnight at room temperature, and labelled as CBNPs/GCE.

Palladium nanoparticles (PdNPs) were electrodeposited on the GCE/CBNPs from a 5 mM palladium chloride solution/electrolyte by running cyclic voltammetry (CV) from −0.3 V to 1.2 V for 20 cycles with continuous stirring with a magnetic stirrer at 200 rpm at 50 mV s^{-1} scan rate.[34] The modified electrode was labelled PdNPs/CBNPs/GCE.

The preparation of the immunosensor was done by immobilising 20 μL of antibody solution of AFP (500 ng mL^{-1}) on the GCE/CBNPs/PdNPs nanocomposite-modified electrode overnight at 4 °C, and subsequently blocked by 0.25% BSA for 4 h to avoid nonspecific binding at the electrode surface. The electrodes were labelled antibody/PdNPs/CBNPs/GCE and BSA/antibody/PdNPs/CBNPs/GCE, respectively. Scheme 1 shows the preparation pathway for the immunosensor.

2.1.3. Electrochemical measurements. Electrochemical characterisation of the modified electrodes was carried out with a 5 mM ferri/ferrocyanide ($[Fe(CN)_6]^{3-/4-}$) redox probe in 0.1 M KCl solution. The following conditions were used: CV – 50 mV s^{-1}; SWV – a pulse amplitude of 0.05 V and a frequency of 25 Hz; EIS – 0.22 V as bias potential (E^o), 100 kHz to 0.1 Hz as the frequency range and 0.01 V as the amplitude.

3. Results and discussion

3.1. Morphological studies

CBNPs are depicted as having spherical particle morphology with some sizes in the sub-100 nm range (Fig. 1A and B). The morphology of the electrodeposited PdNPs was studied on a screen-printed carbon electrode (SPCE). A similar spherical morphology, although smaller in size to that of CBNPs, is seen (Fig. 1C). For CBNPs/PdNPs, the morphology of the individual nanoparticles in the composite is not easily distinguishable owing to similarities in shape (Fig. 1D). However, the EDS of CBNPs/PdNPs shows the presence of palladium and carbon (Fig. 1E). The TEM image shows the nanoparticle morphology of the CBNPs (Fig. 1F) and the hybrid is distinguishable by density of the individual atom (Fig. 1G) – the bigger and less dense sample is the CBNPs, while the smaller and more dense nanoparticle is palladium.

3.2. Electrochemical characterisation

Changes in the peak current and ΔE are indicative of an improved electroactive surface area and variations in the interfacial kinetics of the redox probe electrochemistry at the different interfaces, respectively. The anodic peak current (I_{pa}) and ΔE of each modified electrode is presented in Table 1. Modification with CBNPs (Fig. 2A(b)) brought about an enhancement of the redox current of the redox probe when compared with the bare electrode (Fig. 2A(a)). The increase can be ascribed to the larger surface area created by the CBNPs, allowing for more oxidation and reduction of ferrocyanide molecules per unit time. Upon the electrodeposition of PdNPs to form the CBNPs/PdNPs, a marked increase in current from 0.23 mA (CBNPs) to 0.32 mA (CBNPs/PdNPs) was observed (Fig. 2A(c)), and this also corresponds to the lowest ΔE of 75 mV. This change is attributed to the further increase in surface area of the electrode, possible electrocatalysis as a result of the PdNPs, and increase in the rate of electron transfer (reduced ΔE). As expected, the immobilisation of the AFP antibody on the CBNPs/PdNPs-modified electrode (Fig. 2A(d)) caused a drop in the current because the poorly conducting biomaterial slows down the electron transfer. The effect of blocking the non-AFP antibody-immobilised locations on the electrode surface by the BSA is noticeable by the 82% current reduction and increase in ΔE, as compared to the GCE/CBNPs/PdNPs platform, seen in Fig. 2A(e) and Table 1. The BSA hinders the electron transfer rate at the ferrocyanide/electrode interface.

The EIS (Fig. 2B) was fitted using a Randles equivalent circuit (Fig. 2B inset) consisting of solution resistance (R_s), Warburg

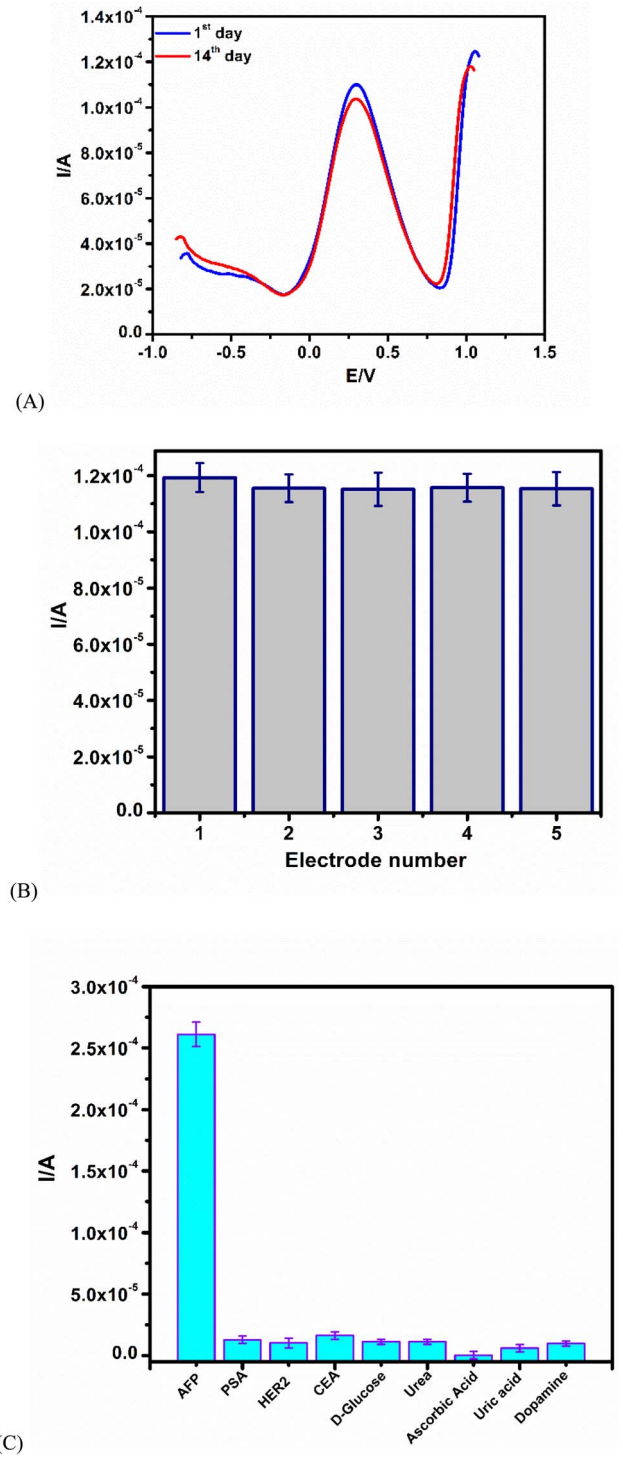

Fig. 5 (A) Stability test: first day to the fourteenth day by SWV in 5 mM ferriferrocyanide in 0.1 M KCl solution. (B) Reproducibility studies. (C) Selectivity result of the proposed immunosensor in the presence of interferents.

impedance (Z_w), charge transfer resistance (R_{ct}), and double-layer capacitance (C_{dl}). The data derived from the equivalent circuit are listed in Table 1. The trend in the R_{ct} values agrees with the result from CV: the lowest R_{ct} (5.78 Ω) at CBNPs/PdNPs corroborates the highest current in Fig. 2B(c) (Table 1). Immobilisation of the AFP antibody on the modified electrode (Fig. 2B(d)) increased the R_{ct} to 18.16 Ω (Table 1), and blocking with BSA (Fig. 2B(d)) resulted in a further increase in R_{ct} to 44.76 Ω (Table 1). It is expected that the biomolecules – AFP and BSA – will block sites on the CBNPs/PdNPs, which will impede the flow of electrons. Of note is the marked change in R_{ct} when the GCE/CBNPs is compared with the CBNPs/PdNPs platform. This change depicts a synergistic combination of the two nanoparticles, which brings about an increase in the rate of electron transfer and the surface area. These enhancements will be beneficial for the immunosensor readout. The bare GCE had the largest charge transfer resistance, as indicated in the Nyquist plot inset in Fig. 2B.

A linear regression equation of $Y\,(\mathrm{A}) = 2.3750x + 1.5940$ and a correlation coefficient of $(R^2) = 0.9969$ were obtained from the scan rate study of the CBNPs/PdNPs/antibodies/BSA (the immunosensor). The obtained linear relationship between the peak current and the square root of the scan rates shows that the kinetics of electron transfer is a diffusion-controlled process (plot not shown). The obtained linearity forms the premise for the quantification of AFP by the immunosensor.

3.3. Optimisation of conditions of the immunosensor

It is important to optimise the conditions necessary for the best immunosensor readout. We investigated incubation temperatures from 20 to 50 °C in 100 ng mL^{-1} of AFP antigen. The most favourable temperature condition for the immunocomplex formation (antibody–antigen interaction) was at 30 °C (Fig. 3A). For incubation time, the highest current peak height at 30 min was chosen (Fig. 3B).

3.4. Electrochemical detection of AFP

Control experiments using various immunosensor platforms were conducted for the detection of AFP antigen to show the performance of the nanocomposite platform. The lowest current response is observed at the bare GCE (Fig. 4A(a)), while the positive effect of modification is seen from the enhancement of the peak (with reference to bare GCE) on all of the modified electrodes. Fig. 4A(d), the nanocomposite platform CBNPs/PdNPs, shows the highest current response. This shows the beneficial effect of combining the two nanoparticles as the immunosensor platform.

The immunosensor was utilized in the analysis of various concentrations of the AFP antigen with SWV and EIS as interrogating tools. For SWV, an increase in the concentration of the antigen increases the amount of antigen bound to the antibody. The increase in the density of antigen–antibody immune-complex creates an insulating or blocking effect towards the approach of the redox probe, and thus decreases the amount of redox electron transport at the interface of the immunosensor and the redox probe in solution – this is a signal-off approach. The calibration curve (Fig. 4B inset) of the AFP concentration is linear (from 0.005 to 1000 ng mL^{-1}), with a regression equation of $Y\,(\mathrm{A}) = 6.0109x + 6.3975$ and a correlation coefficient of 0.9925. A good limit of detection of 0.0039 ng mL^{-1} was

Table 3 Quantification of AFP in human serum samples

Serum sample number	Addition content (ng mL^{-1})	Amount detected (ng mL^{-1})	RSD (%, $n = 6$)	Recovery (%)
1	5.0	5.06, 5.05, 5.03, 4.99, 4.98	0.7603	100.5
2	50.0	49.90, 49.97, 50.00, 50.04, 50.03	0.1089	99.98
3	100.0	100.01, 99.91, 100.06, 100.05, 99.90	0.0778	99.99

achieved for the SWV from $3 \times \frac{SD}{m}$, where SD is the standard deviation of the blank and the m is the gradient of the calibration curve.

The EIS measurement of the biorecognition between the antigen–antibody is a direct proportionality between R_{ct} and the concentration of AFP with a linear AFP concentration range from 0.005 to 1000 ng mL^{-1}. An average error of 6.5% (for R_{ct} fitting), a regression equation of $Y\ (\Omega) = 39.0324x + 1.0846$, a correlation coefficient of 0.9861 (Fig. 4C inset-linear fit) and a detection limit of 0.0131 ng mL^{-1} were obtained. The results demonstrate that the immunosensor showed excellent sensitivity towards the detection of AFP.

The limits of detections from SWV and EIS are of analytical significance since the minimum AFP concentration in the human body is expected to be about 25 ng mL^{-1}. The fabricated immunosensor was compared to other immunosensors reported in the literature, and the methods for the detection used are highlighted in Table 2. The proposed immunosensor has a lower detection limit and a simple fabrication strategy in comparison to other immunosensors.

3.5. Stability, reproducibility, and selectivity studies

SWV was employed to run the proposed immunosensor on day 1 and day 14 (after storage at 4 °C in a refrigerator) with an AFP concentration of 10 ng mL^{-1}. The immunosensor still retained its bioactivity after 14 days. The total loss in signal was about 7.2%, indicating good stability (Fig. 5A). The reproducibility study of the immunosensor was tested using 5 different fabricated GCEs, and tested independently at an AFP concentration of 10 ng mL^{-1}. A relative standard deviation of 5.60% shows that the immunosensor is reproducible (Fig. 5B).

The selectivity study involves the use of different interference agents, such as HER2, CEA, PSA, urea, ascorbic acid, D-glucose, uric acid, and dopamine. The AFP antigen (10 ng mL^{-1}) was incubated in the presence of interfering agents (Fig. 5C). The effect of all of the interfering agents on the immunosensor showed less than 12.5% interference, an indication of good selectivity.[40,43,44]

3.6. Application in human serum samples

The immunosensor was applied in the detection of AFP in a more complex matrix human serum. The human serum was diluted in the ratio of 1 : 100 with phosphate buffer solution using the standard addition technique. The sample was analyzed five times with different concentrations of AFP (5.0, 50.0 and 100.0 ng mL^{-1}) added to the diluted human serum. A relative standard deviation of 0.0778–0.7603% and percentage recoveries in the range of 99.98–100.05% were calculated (Table 3). These good percentage recoveries highlight the potential of the immunosensor for real life applications.

4. Conclusion

An immunosensor for the label-free detection of an alpha-fetoprotein cancer biomarker has been prepared from a novel synergistic combination of two unique, inexpensive, and conductive nanomaterials, namely the carbon black nanoparticles and palladium nanoparticles. The hybrid CBNPs/PdNPs enhanced the electrochemical performance of GCE towards a ferrocyanide redox probe in comparison to the CBNPs and PdNPs. The immunosensor has the advantage of the dual detection method of SWV and EIS with analytically relevant limits of detection of 0.0039 ng mL^{-1} (SWV) and 0.0131 ng mL^{-1} (EIS) with a broad linear range from 0.005 ng mL^{-1} to 1000 ng mL^{-1} AFP concentration. The immunosensor was reproducible, stable, and selective in the presence of interfering species. The potential for real sample applications was supported by the good recovery values in human serum matrix.

Author contributions

Foluke O. G. Olorundare: conceptualisation, formal analysis, methodology, investigation, writing – original draft. Dimpo S. Sipuka: methodology, visualization, writing – review and editing. Tsholofelo I. Sebokolodi: methodology, visualization, writing – review and editing. Tetsuya Kodama: visualization, writing – review and editing. Omotayo A. Arotiba: conceptualisation, methodology, visualization, supervision, funding acquisition, writing – review, and editing. Duduzile Nkosi: conceptualisation, methodology, visualization, supervision, project administration, funding acquisition, writing – review, and editing.

Conflicts of interest

The authors declare no conflict of interest.

Acknowledgements

We acknowledge the National Research Foundation NRF, South Africa (CPRR Grant No. 118546); the Center for Nanomaterials Science Research, University of Johannesburg South Africa, and

the Faculty of Science University of Johannesburg, South Africa for funding this research.

References

1 T. Feng, Y. Wang and X. Qiao, *Electroanalysis*, 2017, **29**, 662–675.
2 R. L. Siegel, K. D. Miller, H. E. Fuchs and A. Jemal, *Ca-Cancer J. Clin.*, 2022, **72**, 7–33.
3 E. Finestone and J. Wishnia, *S. Afr. J. Oncol.*, 2022, **6**, 7.
4 R. Sharma, M. Nanda, C. Fronterre, P. Sewagudde, A. E. Ssentongo, K. Yenney, N. D. Arhin, J. Oh, F. Amponsah-Manu and P. Ssentongo, *Trop. Front. Public Health*, 2022, **10**, 1–14.
5 D. Sadighbayan, K. Sadighbayan, M. R. Tohid-Kia, A. Y. Khosroushahi and M. Hasanzadeh, *TrAC, Trends Anal. Chem.*, 2019, **118**, 73–88.
6 H. Boyacıoğlu, B. B. Yola, C. Karaman, O. Karaman, N. Atar and M. L. Yola, *Appl. Surf. Sci.*, 2022, **578**, 152093.
7 C. Shen, L. Wang, H. Zhang, S. Liu and J. Jiang, *Front. Chem.*, 2020, **8**, 589560.
8 M. Giannetto, L. Elviri, M. Careri, A. Mangia and G. Mori, *Biosens. Bioelectron.*, 2011, **26**, 2232–2236.
9 J. Chen and G.-C. Zhao, *Biosens. Bioelectron.*, 2017, **98**, 155–160.
10 S. A. Zaidi, F. Shahzad and S. Batool, *Talanta*, 2020, **210**, 120669.
11 J. Upan, N. Youngvises, A. Tuantranont, C. Karuwan, P. Banet, P.-H. Aubert and J. Jakmunee, *Sci. Rep.*, 2021, **11**, 1–9.
12 F. Fan, H. Shen, G. Zhang, X. Jiang and X. Kang, *Clin. Chim. Acta*, 2014, **431**, 113–117.
13 P. Preechakasedkit, W. Siangproh, N. Khongchareonporn, N. Ngamrojanavanich and O. Chailapakul, *Biosens. Bioelectron.*, 2018, **102**, 27–32.
14 C. Chen, J. Zhao, Y. Lu, J. Sun and X. Yang, *Anal. Chem.*, 2018, **90**, 3505–3511.
15 X. Zheng, X. Hua, X. Qiao, F. Xia, D. Tian and C. Zhou, *RSC Adv.*, 2016, **6**, 21308–21316.
16 T. Wangkam, K. Boonperm, P. Khomkrachang, T. Srikhirin, V. Praphanphoj, B. Sutapan, A. Somboonkaew and R. Amarit, *Adv. Mater. Res.*, 2016, **1131**, 84–87.
17 J. Li, D. Liu, D. Zhou, L. Shao, X. Chen and H. Song, *Talanta*, 2021, **225**, 122074.
18 Y. Jiang, D. Liu, Y. Yang, R. Xu, T. Zhang, K. Sheng and H. Song, *Sci. Rep.*, 2016, **6**, 1–8.
19 Y. Wang, Y. Zhang, D. Wu, H. Ma, X. Pang, D. Fan, Q. Wei and B. Du, *Sci. Rep.*, 2017, **7**, 1–10.
20 C. Karaman, Ö. S. Bölükbaşı, B. B. Yola, O. Karaman, N. Atar and M. L. Yola, *Anal. Chim. Acta*, 2022, **1200**, 339609.
21 O. Karaman, N. Özcan, C. Karaman, B. B. Yola, N. Atar and M. L. Yola, *Mater. Today Chem.*, 2022, **23**, 100666.
22 X. Zhang, J. Sun, J. Liu, H. Xu, B. Dong, X. Sun, T. Zhang, S. Xu, L. Xu and X. Bai, *Sens. Actuators, B*, 2018, **255**, 2919–2926.
23 J. Upan, N. Youngvises, A. Tuantranont, C. Karuwan, P. Banet, P.-H. Aubert and J. Jakmunee, *Sci. Rep.*, 2021, **11**, 13969.
24 K. Sheng, W. Liu, L. Xu, Y. Jiang, X. Zhang, B. Dong, G. Lu and H. Song, *Sens. Actuators, B*, 2018, **254**, 660–668.
25 S. Krishnan, X. He, F. Zhao, Y. Zhang, S. Liu and R. Xing, *Anal. Chim. Acta*, 2020, **1133**, 119–127.
26 A.-J. Wang, X.-Y. Zhu, Y. Chen, P.-X. Yuan, X. Luo and J.-J. Feng, *Sens. Actuators, B*, 2019, **288**, 721–727.
27 B. B. Yola, C. Karaman, N. Özcan, N. Atar, I. Polat and M. L. Yola, *Electroanalysis*, 2022, **34**, 1519–1528.
28 V. Mazzaracchio, L. Tshwenya, D. Moscone, F. Arduini and O. A. Arotiba, *Electroanalysis*, 2020, **32**, 3009–3016.
29 G. Evtugyn, A. Porfireva, R. Shamagsumova and T. Hianik, *Chemosensors*, 2020, **8**, 96.
30 K. Meduri, A. Rahimian, R. A. Humbert, G. O. B. Johnson, P. G. Tratnyek and J. Jiao, *Mater. Perform. Charact.*, 2019, **8**, 479–489.
31 A. Yan, B. W. Lau, B. S. Weissman, I. Külaots, N. Y. Yang, A. B. Kane and R. H. Hurt, *Adv. Mater.*, 2006, **18**, 2373–2378.
32 Y. Li, L. Tian, L. Liu, L. Liu, J. Li, Q. Wei and W. Cao, *New J. Chem.*, 2016, **40**, 558–563.
33 M. Ławrywianiec, J. Smajdor, B. Paczosa-Bator and R. Piech, *Food Anal. Methods*, 2017, **10**, 3825–3835.
34 L. Suresh, J. S. Bondili and P. K. Brahman, *Electroanalysis*, 2020, **32**, 1439–1448.
35 R. Shandilya, A. Bhargava, N. Bunkar, R. Tiwari, I. Y. Goryacheva and P. K. Mishra, *Biosens. Bioelectron.*, 2019, **130**, 147–165.
36 U. Jain, M. Khanuja, S. Gupta, A. Harikumar and N. Chauhan, *Process Biochem.*, 2019, **81**, 48–56.
37 L. Wang, T. Meng, L. Liang, J. Sun, S. Wu, H. Wang, X. Yang and Y. Zhang, *Sens. Actuators, B*, 2019, **278**, 133–139.
38 T. R. Tsekeli, T. I. Sebokolodi, D. S. Sipuka, F. O. Olorundare, S. P. Akanji, D. Nkosi and O. A. Arotiba, *J. Electroanal. Chem.*, 2021, **901**, 115783.
39 T. Mushiana, N. Mabuba, A. O. Idris, G. M. Peleyeju, B. O. Orimolade, D. Nkosi, R. F. Ajayi and O. A. Arotiba, *Sens. Bio-Sens. Res.*, 2019, **24**, 100280.
40 A. O. Idris, N. Mabuba and O. A. Arotiba, *Anal. Methods*, 2018, **10**, 5649–5658.
41 C. Zhou, D. Liu, L. Xu, Q. Li, J. Song, S. Xu, R. Xing and H. Song, *Sci. Rep.*, 2015, **5**, 1–7.
42 Y. Niu, T. Yang, S. Ma, F. Peng, M. Yi, M. Wan, C. Mao and J. Shen, *Biosens. Bioelectron.*, 2017, **92**, 1–7.
43 A. O. Idris, N. Mabuba and O. A. Arotiba, *Electroanalysis*, 2018, **30**, 31–37.
44 L. Jothi, S. K. Jaganathan and G. Nageswaran, *Mater. Chem. Phys.*, 2020, **242**, 122514.